Journal of Robotics and Control (JRC)
Volume 6, Issue 4, 2025
ISSN: 2715-5072, DOI: 10.18196/jrc.v6i4.26385

Robust Velocity Control for a Launch Vehicle Erection System

Ahmed K. Saber [1*], Shady A.Maged [2], M. Abdelaziz [3], Mostafa S. Mohamed [4]
[1,2] Mechatronics Engineering Department. Faculty of Engineering, Ain Shams University, Cairo, Egypt
[3] Head of Automotive Engineering Department. Faculty of Engineering, Ain Shams University, Cairo, Egypt
[4] Military Technical College, Cairo, Egypt
Email: [1] 2200049@eng.asu.edu.eg, [2] shady.maged@eng.asu.edu.eg, [3] mohamed_abdelaziz@eng.asu.edu.eg
[4] mostafasaad43@gmail.com
*Corresponding Author

***Abstract*—The design of a launch vehicle erection system requires careful consideration of factors such as load capacity, pressure requirements, actuator type, safety mechanisms, and control strategy. Ensuring precise velocity control is critical, as the system's changing geometry and dynamic behavior influence its loading conditions, stability, and overall performance. This study investigates the velocity control of a hydraulic erection beam using a proportional directional control valve (PDCV). Four control techniques are examined: a classical PID controller, a sliding mode controller (SMC), a model predictive controller (MPC), and a PID controller optimized using the Particle Swarm Optimization (PSO) method. The controllers are evaluated through MATLAB/SIMULINK simulations under both undisturbed and disturbed conditions. Simulation results indicate that the classical PID controller struggles with stability under disturbances, while the MPC exhibits slow response times and fails to reach the desired position. The integration of PSO further degrades performance by introducing instability. In contrast, the SMC demonstrates superior robustness, achieving minimal response variation across all conditions. Comparative experiments validate these findings, confirming that SMC offers the best balance of precision, reliability, and disturbance rejection. These results highlight that SMC is the most effective control technique for real-world hydraulic erection systems, ensuring high stability, accuracy, and operational reliability.**

Keywords*—*Launch Vehicle Erection System (LVES); Velocity Control; Electro-Hydraulic System (EHS); Proportional Directional Control Valve (PDCV); PID Control; Sliding Mode Control (SMC); Model Predictive Control (MPC); Particle Swarm Optimization (PID-PSO)

I. Introduction

Launch vehicle erection systems (LVES) are used in numerous sectors, requiring precise lifting [1], positioning, and assembly of substantial components. To raise and place significant components, LVES utilize hydraulic pressure to generate force supplied through cylinders [2]. Such systems' complicated control and stability handle various problems, such as nonlinear dynamics [3], external disturbances [4], sensor inaccuracies, and time-varying parameters [5]. Electrohydraulic control techniques monitor and regulate hydraulic fluid flow to ensure stability [6], meticulousness, and optimal performance despite struggling operating conditions.

In the last decades, Electro-Hydraulic system (EHS) have been widely used in most applications that need high power to perform multifaceted activities with high accuracy and reliability [7]. Therefore, EHS provides a smooth and fast response based on the input action, so it's deployed in high-capacity production lines [8] such as heavy machinery, aerospace, robotics [9], ships, and automotive. EHS integrates hydraulic technology with electronic control to achieve precise and efficient motion and force regulation. The electro-hydraulic control systems (EHCS) empower the electrical signals to control the operation of hydraulic components such as pumps, valves, and actuators [10], facilitating real-time adjustments in pressure, flow rate, and motion. EHS keep developing due to the increasing demand for more dependable, efficient, and automated systems in sectors. This results in new control techniques, sensor technologies, and energy management ideas. EHCS apply several approaches and strategies to provide exact control of hydraulic actuators. The commonly utilized methods in EHCS are Proportional-Integral-Derivative (PID) controller [11], Adaptive Control, Fuzzy Logic Control [12], Sliding Mode Control (SMC), Hybrid Control [13], and Model Predictive Control (MPC). These methods are investigated and analyzed to select the most appropriate method for this work in section 2. Because of their complicated character, LVES provide significant problems for EHCS [14]. The modeling and control of the system suffer from the nonlinear interactions among hydraulic pressure, actuator movement, and load. The robustness of the control method is challenged by disturbances and external loads [15] leading to erroneous positioning and unstable system behavior. The dynamics of LVES are time-varying and driven by alterations in hydraulic resistance, system inertia, and friction [16]. Accurate feedback is necessary for effective control as high-load systems are usually affected by noisy sensor data, measurement precision limitations, and response delays.

The complex hydraulic systems employ the Proportional Directional Control Valve (PDCV) to regulate the flow and rate of hydraulic fluid. Compared with the standard DCVs [17], proportional valves provide variable flow control based on an input signal, facilitating enhanced control precision and fast response. The (PDCV) [18] include hydraulic systems that use proportional solenoids or electromagnetic coils to precisely regulate the flow rate of hydraulic fluid to actuators, such as hydraulic cylinders. PDCV drives allow precise control of actuator position, speed, or force by adjusting the electrical input to the solenoid, which modulates the valve opening and, thus, the fluid flow rate. The suitable choice of hydraulics in LVES and the integration of PDCVs can increase performance and dependability.

The control action is applied through various control elements in the hydraulic circuit through PDCV, pressure relief valve, flow control valves [19], throttle valves, counterbalance valve, and so on. Sliding Mode Control (SMC) is one of the most widely used robust control algorithms, offering a significant advantage in handling linear and nonlinear systems, especially in the presence of uncertainties. Integrating SMC with a system ensures a fast and accurate response while reducing noise [20]. Due to these advantages, SMC is a preferable control choice compared to conventional PID controllers.

Meanwhile, hydraulic components are incorporated with control systems, an extensive load erection system can be designed and validated, ensuring safety, accuracy, and stability during heavy lifting operations [21]. This design process integrates validation simulation, control algorithm development, and hydraulic system analysis. Determining the suitable cylinder size and stroke length is necessary in system design to control the predicted load and the industrial safety standards [16]. The proper selection of precise DCV, actuation, and accurate sensors to monitor hydraulic pressure and provide reliable response. Developing a mathematical model guarantees firm hydraulic system control incorporating control inputs, predicted loads, hydraulic pressure, actuator movement, and load dynamics. The flexibility and operational integrity of the model are validated using MATLAB/Simulink simulations under both stationary and dynamic settings [22]. This simulation ensures the system's response and stable lifting and positioning of the load under varying conditions. The main contribution of this paper can be summarized as follows:

- Multiple control strategies for regulating pressure in the erection system were designed, including classical PID, (SMC), (MPC), and PID were optimized with Particle Swarm Optimization (PID-PSO).
- A nonlinear model of the erection system and its hydraulic circuit has been constructed for controller design purposes.
- Control techniques are assessed based on critical parameters, including rising time, settling time, mean error, and resilience against shocks and noise [23].
- Practical Verification includes simulations using MATLAB/Simulink to validate the proposed models and control strategies under nominal and disturbed conditions.

This paper is structured as follows: the first section introduces the launch vehicle erection system and EHS, as well as their methods, advantages, and applications: the (PDCV) and different control methods to control the actuators. The second section presents the EHSs, including their ability to achieve precise control of hydraulic actuators. The third section presents the Control Approach of four control techniques on a nonlinear system to select the best one for designing a more robust control system and compares the four control techniques. The fourth section presents the practical verification of the selected control technique to validate the proposed control strategies under nominal and disturbed conditions. The fifth system is the conclusion and future work.

II. METHODS

To perform the control process on the erection mechanism, Fig. 1 illustrates the following four control techniques [24] that will be utilized in the research.

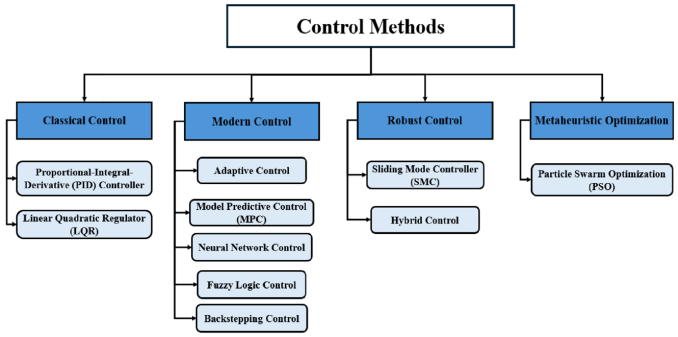

Fig. 1. Control Methods

The study explores four distinct control approaches for regulating the angular velocity $(\dot{\alpha})$ of the launch vehicle erection system:

1) Classical Control Technique: A Proportional-Integral-Derivative *(PID)* controller is implemented to regulate the *(PDCV)*, ensuring stable velocity tracking.
2) Modern Control Technique: A Model Predictive Controller *(MPC)* is designed to optimize system performance by predicting future system states and applying control actions accordingly.
3) Robust Control Technique: A Sliding Mode Controller *(SMC)* is applied to the *PDCV* to enhance system robustness against external disturbances and modeling uncertainties.
4) Metaheuristic Optimization-Based Control: A Particle Swarm Optimization *(PSO)*-based *PID* controller is devel-

oped to fine-tune the *PID* parameters, improving response time and minimizing steady-state error.

A. Control Approach

Achieving precise control in hydraulic actuator systems necessitates employing various techniques, each possessing distinct advantages and disadvantages. Selecting the most appropriate technique hinges on specific application requirements, efficiency, and operational constraints. Common control strategies include the Classical (PID) controller , (SMC), (MPC), (PSO), Aaptive Control, Neural Network Control, Fuzzy Logic Control, Back stepping Control, Hybrid Control, and Linear Quadratic Regulator (LQR)

PID control is prevalent in many industrial applications and is easy to utilize. It works well for systems that are well-defined, stable, and have low to moderate complexity [25]. It is also straightforward to tune and consistently performs well. However, the PID controller struggles with disturbances and performs less well in highly dynamic and nonlinear systems. (SMC) is highly robust against external disturbances and parameter uncertainties to handle uncertainties effectively. Fast response times and exact tracking are features of SMC [26], but implementation is complex because the discontinuity of the control signal causes chattering, which causes problems .

Predicting future behavior based on present and past data helps (MPC) to offer ideal control. It is successful for systems with complicated dynamics and restrictions and can manage several goals simultaneously. Still, it uses many resources; hence, tweaking values can be difficult and might call for regular updates [27]. (PSO) based PID Controller combines the simplicity of PID control with the global search capabilities of PSO, optimizing control parameters automatically and improving system performance [28]. It's efficient for nonlinear and complex systems. However, it requires intensive resource consumption, and tuning parameters can be challenging and sensitive to initialization conditions.

Adaptive control is optimal for systems experiencing significant variations in load, system dynamics, or external disturbances. This technique can enhance system stability and performance without requiring extensive manual tuning [29]. However, parameter tuning necessitates real-time monitoring and can be computationally intensive. Similarly, neural network control can learn complex and highly nonlinear system behaviours through training, adapting, and generalizing from data. This makes it particularly useful for systems with changing dynamics. Nevertheless, the computational intensity and constraints of real-time applications may present challenges [30]. Tuning network architecture and learning parameters can be complex and time-consuming.

Fuzzy logic control can handle complex, nonlinear relationships without requiring detailed system models. It's robust to disturbances and variations in system parameters, but fuzzy rule design requires expert knowledge [31]. Developing the rule base may require significant time and be less efficient in systems where rapid and accurate response times are essential [32]. Combining the qualities of several control strategies, PID, SMC, MPC, fuzzy logic, etc., hybrid control can maximize their complementary advantages to offer flexibility and adaptation to changing system conditions [33]. One can customize hybrid control to perform best over various running conditions. However, it is computationally difficult; hence, the real-time implementation and adjustment of individual control components provide significant difficulties.

The four optimal approaches for the LVES are (SMC), (MPC), PID, and (PSO)-Based PID controller. SMC exhibits exceptional resilience to disturbances and nonlinearities, rendering it suitable for dynamic and uncertain contexts. MPC provides optimal regulation for intricate systems with several restrictions, whereas (PID) controller offers simplicity, ease of tuning, and effective performance for stable systems, making it widely applicable in industries. However, it struggles with highly nonlinear systems. PSO-based PID offers comprehensive optimization for system calibration, harmonizing performance and efficiency. These approaches are chosen for their capacity to meet the stringent demands of heavy-load systems, including robustness, precision, and adaptability.

Designing an accurate and effective (LVES) involves a combination of theoretical analysis, simulation, and experimental validation [34]. Nonlinear systems present significant challenges in (LVES) due to complexities in modeling nonlinearities like hydraulic component behavior, friction, and load characteristics [35]. Addressing these challenges requires accurate nonlinear modeling, robust control design, and extensive simulation and testing. Strategies include advanced modeling techniques, incorporating uncertainty handling mechanisms, and implementing safety interlocks to mitigate risks associated with unpredictable behavior [36].

Fig. 2 shows the systematic approach to design a hydraulic system [37]. The initial step of selecting hydraulic components involves choosing suitable components like pumps, valves, cylinders, and accumulators based on the system's requirements. Identifying load characteristics such as mass, inertia, and friction is crucial for determining the necessary force and speed for the hydraulic system. Operational and safety constraints include operating pressure, temperature limits, and safety requirements to ensure the system's reliability and prevent hazards. Erection system modeling consists of a mathematical or computational model of the system created to predict its behavior and performance [38]. This model should account for the load characteristics, hydraulic components, and control strategy. (PDCV) and Hydraulic Cylinders are specific components of the system. (PDCV) regulate fluid flow, while the hydraulic cylinder converts hydraulic pressure into linear motion. Control strategy selection involves choosing the

appropriate control algorithm to regulate the system's behavior. MATLAB/Simulink will be used to define the most suitable control strategy implementation and practical verification to validate the proposed models and control strategies under nominal and disturbed conditions [39]. Finally, select the optimal controller based on performance, robustness, and safety. The aforementioned design ensures reliable performance under varying operational conditions and enhances overall system safety and efficiency [40].

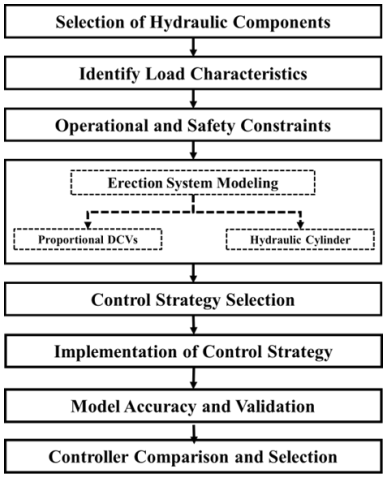

Fig. 2. Flowchart of designing an accurate and effective launch vehicle erection system.

B. System Terminology

The development of non-linear models for the hydraulic circuit and erection system begins with a comprehensive process of system modeling and simulation [41]. The first step involves analyzing the components and dynamics of the hydraulic circuit and erection system. The erection system comprises a hydraulic cylinder, power source, lifting boom, payload, and servo control system [15]. These non-linear models are then used to facilitate designing a suitable control process. Mathematical models are constructed to represent the behavior of every component based on the system analysis [42]. These models are often non-linear due to the complex relationships between variables. Accurate parameter identification of the mathematical model is crucial for its reliability. MATLAB/Simulink is used for numerical simulations to analyze the behavior of the hydraulic circuit and erection system under various operating conditions and validate performance and stability for the non-linear system.

The motion of the hydraulic cylinder connection to the erection angle is theoretically modeled to find the exact correlation between hydraulic actuation and the resultant angular displacement. As shown in Fig. 3, the geometry and forces involved in operating a hydraulic cylinder are used to control the erection system. In this figure, the hydraulic cylinder, the core of the actuation system is labelled with (c), the lifting arm pivots about point (O) is labelled with (a), the payload (erecting structure) is labelled with (GT), and the hydraulic actuation is labeled with (b). The erection angle (α) is the angle between the initial position of the erection system and its current raised position. (O1) is the fixed pivot point for the top of the hydraulic cylinder. (O1') represents a possible alternative position of that point if the cylinder were at a different extension. (Fr) and (Ft) are the forces and the motions.

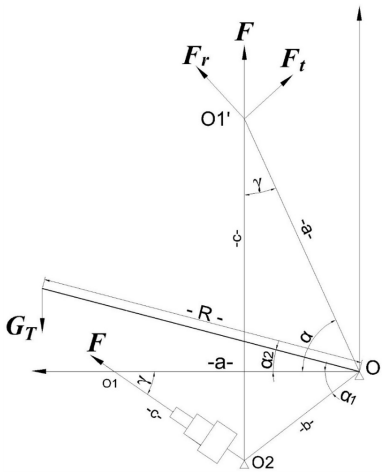

Fig. 3. The erection system cylinder operation diagram.

Fig. 3 shows the hydraulic circuit layout reveals the circuit components that control the pressure entering the hydraulic cylinder. And the elements of the hydraulic circuit are shown in Fig. 4.

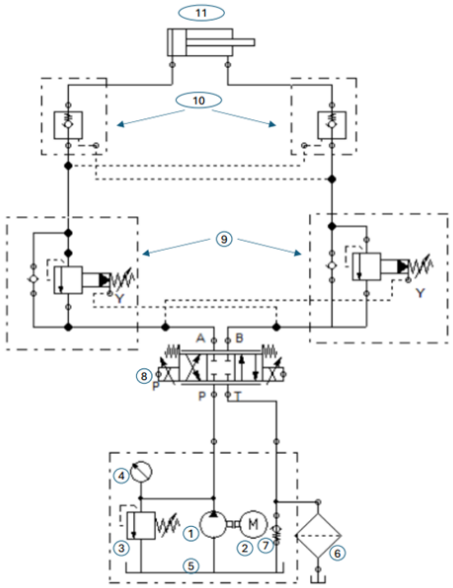

Fig. 4. Schematic representation of the electro-hydraulic proportional system.

The beam $\overline{(O\,O_1)}$ starts motion at $\alpha = \alpha_2$, begins rotation about point O, and ends its motion when α reaches $90°$.

Where: (1) REXROTH 0510-425-011 Gear Pump, (2) electric motor Ybx3 Series Ybx3-160m-4 11kw, (3) Pressure relief valve ATOS ARE-15/250, (4) WIKI pressure gauge, (5) Hydraulic reservoir, (6) Return filter RFM-40, (7) VOSS Check valve, (8) Proportional direction control valve (PDCV) PARKER series D1FP spool type (E01/E50), (9) PARKER–CB series counterbalance valve, (10) ATOS KR-013/33Pilot operated check valve, (11) Double acting cylinder trunnion mount. Using hydraulic oil ISO VG 68.

At the core of our setup, here's a concise summary of the hydraulic system components:

A REXROTH 0510-425-011 gear pump (1), driven by an 11kW Ybx3-160m-4 electric motor (2), delivers pressurized ISO VG 68 hydraulic oil from a hydraulic reservoir (5) to power the system. System pressure is regulated by an ATOS ARE-15/250 pressure relief valve (3), while a WIKI pressure gauge (4) monitors pressure fluctuations. A VOSS check valve (7) operates in parallel with the RFM-40 return filter (6), allowing oil to bypass the filter in case of clogging, ensuring uninterrupted flow back to the reservoir. A PARKER D1FP spool-type proportional directional control valve (PDCV) (8) precisely modulates oil flow to control the velocity and direction of movement [43]. PARKER CB-series counterbalance valves (9) provide stability by holding pressure and preventing overrun due to external forces to prevent uncontrolled actuator movement under load [44].

This inhibits unwanted motion and guarantees accurate load control, especially in applications which require for stationary holding under changing loads and controlled lowering. which also allow for smooth, targeted actuation, only unlock with pilot pressure, and prevent drift cylinders caused by leakage, and improve system efficiency, safety, and load stability when used in conjunction with counterbalance valves. ATOS KR-013/33 pilot-operated check valves (10) (a hydraulic lock valve is utilized in the circuit to lock the erection mechanism at zero erection angle and 90 ° erection angle or at any emergency stop or leakage occurs) allow load-holding by locking hydraulic pressure in the actuator until a pilot signal is received [45]. This prevents unintended motion and ensures precise load control, particularly in applications requiring controlled lowering and stable holding under variable loads. Additionally, they avoid drift cylinder due to leaks, unlock only with pilot pressure, and enable smooth, deliberate actuation. Combined with counterbalance valves, they enhance load stability, safety, and overall system efficiency [46].

The trunnion-mounted double-acting hydraulic cylinder (11) efficiently converts hydraulic energy into mechanical motion while benefiting from the stability provided by counterbalance and pilot-operated check valves [47]. This system enhances efficiency, reliability, and operational safety, which is required by integrating proportional control, counterbalance mechanisms, and pilot-operated safety features.

C. Pre-Execution Considerations

Before executing the hydraulic circuit, the following factors must be carefully evaluated:

1) Friction Considerations: The friction force within the hydraulic cylinder is considered negligible due to the low surface roughness between the piston and the cylinder bore [48].
2) Oil Stiffness and Compressibility Effects: The bulk modulus of ISO VG 68 hydraulic oil, enhanced with anti-compressibility additives, improves oil stiffness [49]. With $\beta = 1.9$ GPa and the replacement of flexible hoses with steel tubing, the system achieves high stiffness, minimizing compressibility effects at the working pressure 140 bar.
3) Oil Compressibility at Piston Cap and Rod Side:
   - Step 1: Piston Side Volume Calculation The piston side volume is calculated using the piston area and the stroke length:

$$A_p = \frac{\pi}{4}D^2 = \frac{\pi}{4}(0.210)^2 = 0.0346 \text{ m}^2$$

$$V_p = A_p \times L = (0.0346) \times (0.70) = 0.0242 \text{ m}^3$$

   - Step 2: Rod Side Volume Calculation The rod side volume is calculated using the effective annular area:

$$A_r = \frac{\pi}{4}(D_o^2 - D_i^2) = \frac{\pi}{4}(0.115^2 - 0.060^2) = 0.0077 \text{ m}^2$$

$$V_r = A_r \times L = (0.0077) \times (0.70) = 0.0054 \text{ m}^3$$

   - Step 3: Compressed Volume Calculation The compressed volume due to oil compressibility is given by [50]:

$$V_c = \frac{P \times V}{\beta}$$

Compressed Volume at Piston Side:

$$V_{cp} = \frac{(14 \times 10^6) \times (0.0242)}{1.9 \times 10^9} = 178.2 \text{ mL}$$

Compressed Volume at Rod Side:

$$V_{cr} = \frac{(14 \times 10^6) \times (0.0054)}{1.9 \times 10^9} = 39.8 \text{ mL}$$

Total Compressed Volume:

$$V_{\text{total}} = V_{cp} + V_{cr} = 178.2 + 39.8 = 218.0 \text{ mL}$$

- Step 4: Response Lag Time Calculation [51]

$$\text{Response Lag} \approx \frac{V_{\text{total}}}{Q} = \frac{0.000218}{0.0004} = 0.545 \text{ seconds}$$

4) Three-Stage Double-Acting Cylinder Specifications [52]
   - **Stage 1:** Diameter = 210 mm
   - **Stage 2:** Diameter = 170 mm
   - **Stage 3:(Hollow shaft)**
     - Outer Diameter: 115 mm
     - Inner Diameter: 60 mm
5) Buckling Analysis
   - Step 1: Second Moment of Inertia Calculation The second moment of inertia is calculated using:

$$I = \frac{\pi}{64}(D_o^4 - D_i^4)$$

Given:

$$D_o = 0.115 \text{ m}, \quad D_i = 0.060 \text{ m}$$

$$I = \frac{\pi}{64}(0.115^4 - 0.060^4)$$

$$I = \frac{\pi}{64}(1.7474 \times 10^{-3} - 1.296 \times 10^{-4})$$

$$I = \frac{\pi}{64} \times 1.6178 \times 10^{-3}$$

$$I = 9.23 \times 10^{-6} \text{ m}^4$$

   - Step 2: Buckling Load Calculation Using Euler's formula [53]:

$$F_{cr} = \frac{\pi^2 EI}{(KL)^2 \cdot n}$$

Given:

$$E = 210 \times 10^9 \text{ Pa}, \quad I = 9.23 \times 10^{-6} \text{ m}^4$$

$$K = 1 \quad \text{(Fixed-Free Condition)}, \quad L = 0.70 \text{ m}, \quad n = 5$$

$$F_{cr} = \frac{\pi^2 \times (210 \times 10^9) \times (9.23 \times 10^{-6})}{(1 \times 0.70)^2 \times 5}$$

$$F_{cr} = \frac{2.405 \times 10^6}{2.45}$$

$$F_{cr} = 0.274 \text{ MN} = 27.4 \text{ tons}$$

   - Step 3: Buckling Safety Factor

$$SF_{\text{buckling}} = \frac{F_{cr}}{\text{Actual Load}}$$

With Actual Load = 6 tons:

$$SF_{\text{buckling}} = \frac{27.4}{6} = 4.57$$

The updated design ensures improved structural safety, reduced compressibility lag, and optimized hydraulic performance.

While the current study provides a theoretical foundation for the proposed model, a qualitative assessment of the actual object or system is essential to validate its accuracy and applicability; Despite being incapable of directly comparing the model's predictions to actual data at this time, they have been examined within the framework of well-analysed theoretical frameworks and similar systems. In order to overcome this constraint, subsequent research will concentrate on experimental validation by means such as industry partnerships or laboratory studies to gather real-time information Thoroughly comparing the predictions and actual system behavior will ensure the model's trustworthiness for real-world applications. The validation process will also delve deeper into the model's practical consequences, including how it affects mechanical and hydraulic systems' safety, accuracy, and efficiency.

D. Erection Mechanism Mathematical Modelling

The erection system forces and moments involved in lifting and rotating components, ensuring safety and stability throughout the control design of the erection process. Equation (1) represents the rotational equilibrium of the erection system. Equation (2) shows how the total moment during the erection is the sum of the gravitational moment and any additional moments. Equation (3) calculates the gravitational moment based on the weight of the structure being erected, the distance from the pivot, and the inclination angle. Equation (4) describes how external forces, such as wind or additional loads applied at an angle, contribute to the moments acting on the system [54]. Equation (5) combines all components to express the net effect on angular acceleration during the erection process.

$$\sum M = J\ddot{\alpha} \tag{1}$$

$$M = M_G + M_Q = J\ddot{\alpha} \tag{2}$$

$$M_G = G_T \cdot R \cdot \cos(\alpha) \tag{3}$$

$$M_Q = Q \cdot a \cdot \sin(\gamma) \tag{4}$$

$$J\ddot{\alpha} = G_T \cdot R \cdot \cos(\alpha) + Q \cdot a \cdot \sin(\gamma) \tag{5}$$

The relation between hydraulic force F and erection angle α after neglecting wind effect due to its small value corresponding to the force acting will be:

$$F = J\ddot{\alpha} + \frac{G_T \cdot R \cdot \cos(\alpha_1 + \alpha)}{a \cdot b \cdot \sin(\alpha_1 + \alpha)} \cdot \sqrt{a^2 + b^2 - 2 \cdot \cos(\alpha_1 + \alpha)} \tag{6}$$

where F represents the total force acting on the system, $J\ddot{\alpha}$ represents the inertial force resulting from angular acceleration, G_T is the gravitational force (weight), R is the distance from the pivot point to the center of mass, $(\alpha_1 + \alpha)$ is the gravitational moment angle, a is the lifting arm length, b is the hydraulic actuation. So, the relation could be written as:

$$\ddot{\alpha} = \frac{1}{J}\left(Q - \frac{G_T \cdot R \cdot \cos(\alpha_1+\alpha)}{a \cdot b \cdot \sin(\alpha_1+\alpha)} \cdot\sqrt{a^2+b^2-2\cdot a\cdot b\cdot\cos(\alpha_1+\alpha)}\right) \quad (7)$$

The system parameters for erection system simulation are defined in Table 1. These parameters are utilized for developing a control strategy to precisely adjust the hydraulic force (F) to achieve the desired lifting motion (α) despite the launch vehicle and inertia.

E. Proportional Directional Control Valve (PDCV) Model

A proportional Directional Control Valve (PDCV) is a type of hydraulic valve that allows for precise control of fluid flow and direction [55]. The primary purpose of proportional directional control valves PDCV is to control the flow direction and flow rate. it is used to control fluid flow rate by varying flow passage size via a restrictor. PDCVs are widely used in industrial applications because of the possibility of continuous direction and flow rate control. And are often use low-power control signals, which offer precise and programmable control, making them versatile and efficient for controlling the flow rate and direction of the hydraulic fluid [56]. The PARKER series D1FP spool type (E01/E50) is a type of PDCV designed for precise control of hydraulic systems selected for this study. It offers high dynamic performance and high flow rates, excellent pressure handling, and defined spool positioning ensuring safety and reliability. It will be studied as a PDCV valve for controlling beam erection [57]. And its frequency behaviour is shown in valve manual arises in second order linear model as following: The configuration of the valve is shown in equations from 8-10. Equation 8 presents the transfer function of the valve, equation 9 relate the actual flow rate and control signals, equation 10 provides numerical values for the parameters.

$$\frac{Q\%}{V\%} = \frac{w_n^2}{s^2+2\zeta w_n s + w_n^2} = \frac{Q_{\max}}{Q}\cdot\frac{V}{V_{\max}}\cdot\frac{w_n^2}{s^2+2\zeta w_n s+w_n^2} \quad (8)$$

$$\frac{Q}{V} = \frac{Q_{\max}}{V_{\max}}\cdot\frac{w_n^2}{s^2+2\zeta w_n s+w_n^2} \quad (9)$$

From the valve manual, the maximum flow rate achieved at a pressure of 140 bar is equal to 60 L/min with a maximum voltage input of +10V. The natural frequency is given as $\omega_n =$ 60 Hz with a damping ratio of $\zeta = 0.707$, as shown in the following figure.

$$\frac{Q}{V} = \frac{60}{10}\cdot\frac{(120)^2}{s^2+\sqrt{2}(120\pi)s+(120\pi)^2} = \frac{6\cdot(120)^2}{s^2+\sqrt{2}(120\pi)s+(120\pi)^2} \quad \text{(l/min)/V} \quad (10)$$

Where $Q\%$ is the percentage of the maximum flow rate, $V\%$ is the percentage of the control signal (input voltage), ω_n is the natural frequency, ζ is the damping ratio, and s is the complex frequency variable in the Laplace domain. For this research, the PDCV parameters are defined list of abbreviation to design appropriate control strategies.

The relationship between flow rate and outlet pressure in the Pressure Drop Compensated Valve (PDCV) is derived from the orifice flow equation, as shown in Equation (11). The flow rate is determined by the square root of the pressure differential. The flow rates Q_1 and Q_2 for the PDCV are given as:

$$Q_1 = cA_1\sqrt{\frac{2\Delta P_1}{\rho}} = cA_1\sqrt{\frac{2(P_s-P_c)}{\rho}} \quad (11)$$

$$Q_2 = cA_2\sqrt{\frac{2\Delta P_2}{\rho}} = cA_2\sqrt{\frac{2P_r}{\rho}} \quad (12)$$

Where: Q_1 and Q_2 are the flow rates entering and exiting the PDCV, respectively, c is the flow coefficient, A_1 and A_2 are the cross-sectional areas of the orifice, ΔP_1 and ΔP_2 are the pressure drops across the metering orifice and outlet section, respectively, P_s is the supply pressure, P_c is the control pressure, ρ is the fluid density.

Rearrange Eqs. (11) and (12), then we have:

$$P_r = \frac{\rho}{2}\left(\frac{Q_2}{CA_1}\right)^2 \quad (13)$$

$$P_c = P_s - \frac{\rho}{2}\left(\frac{Q_1}{CA_1}\right)^2 \quad (14)$$

$$F = P_cA_c - P_rA_r \quad (15)$$

F. Controllers design and simulation

The controller's mission is to control the beam's angular velocity according to a reference value, controlling the time of erection and the velocity of beam erection through the signal applied to (PDCV) as input [58]. Fig. 5 illustrates the steps of the control system design.

Selecting the control method that best meets the robust control design requires considering factors like robustness's importance, system nonlinearities' level, and available computational resources. Four control methods are selected to determine the most appropriate method for the erection system design: Classical PID Control, (SMC), (MPC), and (PID-PSO). These

four methods cover a range of control strategies with varying levels of complexity and capabilities.

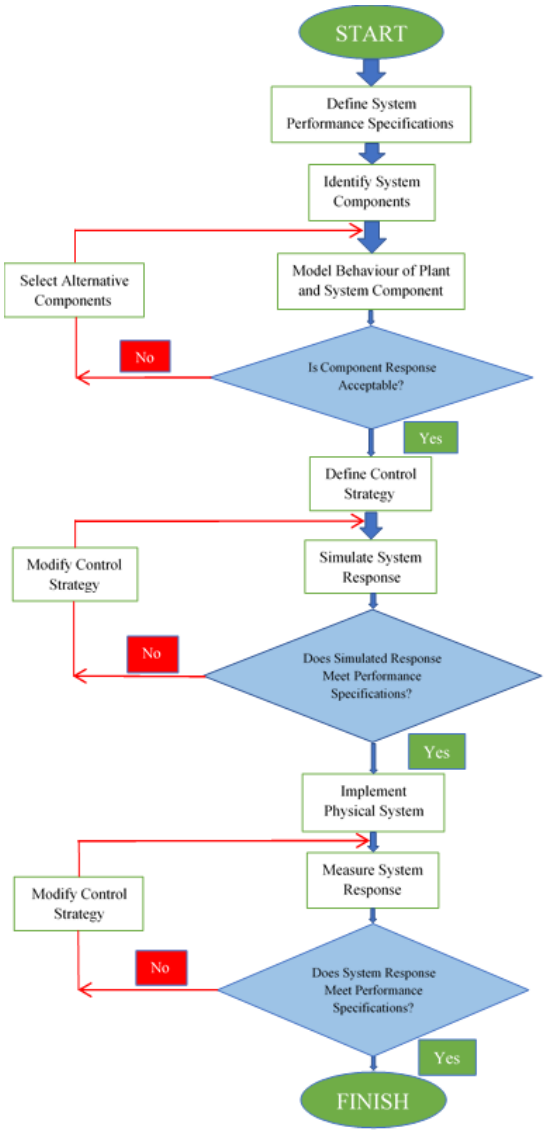

Fig. 5. Steps in the Design of a Control System

1) Model Predictive Control System Simulation: Model predictive control (MPC) is a highly adaptable and efficient control approach effectively utilized in various complex applications, including multi-input, multi-output, delay-afflicted, unstable, and limited systems [59]. Fig. 6 displays the (MPC) block diagram. which refers to an extensive selection of control techniques that use a process model to derive the control signal via minimizing an objective function rather than a particular control strategy. These design techniques result in linear controllers with ample degrees of freedom and almost identical structures [60]. The concepts that are present in all predictive control families, albeit to varying degrees, are:

- The process output is predicted using an explicit model at future time instants (horizon).
- A control sequence that minimizes an objective function is calculated.

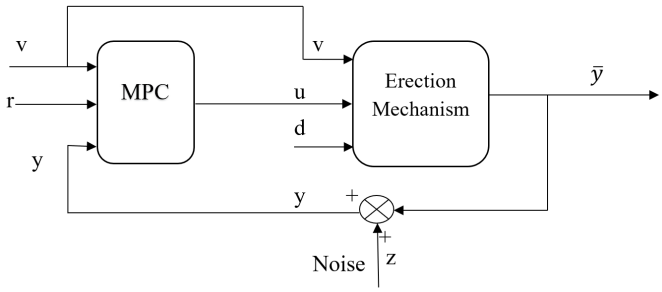

Fig. 6. Basic structure of a Model Predictive Controller

Here is the launch vehicle output: r is the reference angular velocity input, y is the disturbed output, u is the manipulated input to the launch vehicle. The noise is denoted by z, the measured disturbance by v, and the unmeasured disturbance by d. and the MPC family controller's methodology, which is distinguished by the following approach:

1) At each instant kT, it predicts the future outputs for a defined horizon P, also referred to as the prediction horizon, using the process model. These predicted outputs, $y(t+k|t)$ (for $k = 1, \ldots, N$), are crucial as they depend on the known values up to instant kT (past inputs and outputs) and on the future control signals $u(t+k|t)$, where $k = 0, \ldots, N-1$, which are those to be sent to the system and to be calculated. (The notation $(t+k|t)$ indicates the value of the variable at the instant $(t+k)$ calculated at instant t.)
2) The set of future control signals is calculated by optimizing a predetermined criterion to keep the process as close as possible to the reference trajectory $r(t+k)$ (which can be the set point itself or its approximation). The errors between the predicted reference trajectory $r(t+k)$ and the predicted output signal $y(t+k|t)$ typically form a quadratic function of this criterion. The control effort and its rate are included in the objective function.
3) The control signal $u(t|t)$ is sent to the process. On the other hand, since $y(t+1)$ is already known at the subsequent sampling instant, step 1 is repeated using this new value, and all the sequences are up-to-date, so the following control signals are rejected. Consequently, the $u(t+1|t+1)$ is computed, which will theoretically differ from the $u(t+1|t)$ due to the new information.

Using the receding horizon concept. The MPC algorithms possess common elements, which are:

- Prediction Model
- Objective Function
- Obtaining the control law

The MPC control characteristics are obviously depicted in Table I.

TABLE I. MPC CONTROL CHARACTERISTICS

Horizon		Constraints			Simulation scenario	
N_u	N_2	DCV input (V)	x1	x2	x1	x2
2	10	$-10 \leq u \leq 10$	$0 \leq \phi \leq 90$	$0 \leq x_2 \leq 2$	Ramp function	Step function

Performing different scenarios on the non-linear model according to Table II, then the results for erection velocity are shown in Fig. 8

TABLE II. MPC DIFFERENT SCENARIOS

Input Weight		Output Weight	
Weight	Rate	x1	x2
16	5	3	1

Based upon this, the final parameters for MPC are shown in Table III.

TABLE III. MPC CONTROL PARAMETERS

MPC Controller Parameter	Value
Prediction Horizon	10
Control Horizon	2
MPC Cost Weights	
Control Action Weight	16
Control Action Rate Weight	5
Output Weightings	3
ECR Weightings	1

Fig. 7 shows the simulation of an MPC controller. It illustrates that the controller utilizes the feedback of angular velocity and then applies the previously mentioned parameters. The stimulation is performed for 2 (°/s) commanded angular velocity.

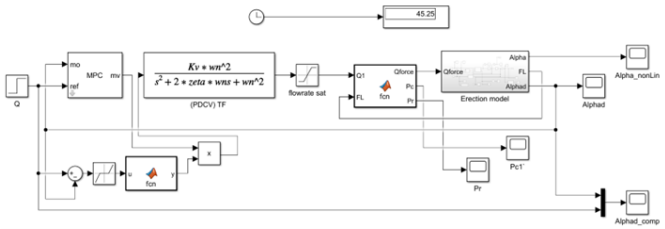

Fig. 7. Classical Control Simulation.

Fig. 8 shows that the plot compares the system's response under Model Predictive Control (MPC) against a constant step reference. The system starts from 0 and gradually increases, trying to reach the command. The response exhibits oscillations, indicating a high-frequency response variation [61]. This suggests that MPC is tracking but with some overshoot or noise, which is evident from the following system response characteristics: the resulting rise time is $t_r = 0.0414$ s, the mean error is $\mu_e = 0.5568°$, and the standard deviation is $\sigma = 0.2776°$.

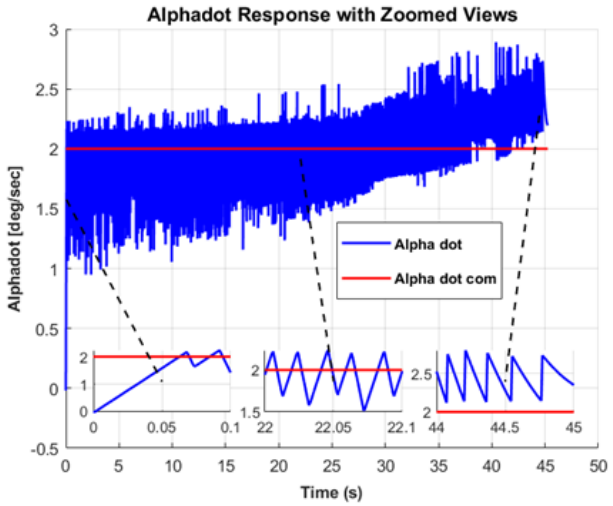

Fig. 8. Simulation Result of MPC Controller by Tuning Prediction Horizon ($\dot{\alpha}$ response).

2) PID-Particle Swarm Optimization (PID-PSO): Particle Swarm Optimization evaluates an objective function at various locations using simple entities called particles [62], which navigate the search space based on their past experiences and interactions with other particles. Each particle updates its position by balancing exploration and exploitation, influenced by its personal best position pi and the global best pg , with added random perturbations. Over time, the swarm converges toward the optimal solution [63].

Each particle in PSO consists of three D-dimensional vectors: position (x_i), velocity (v_i), and personal best position (p_i). The current position is evaluated at each iteration, and if it improves upon p_i, it is updated. The best function value found so far is stored as p_{besti}, and the swarm's best solution is g_{besti} [64]. The velocity update follows:

$$\begin{aligned} v_i(t+1) &= v_i(t) + c_1 \cdot \text{rand}_1 \cdot (x_i(t) - p_i(t)) \\ &\quad + c_2 \cdot \text{rand}_2 \cdot (x_i(t) - p_g(t)), \\ x_i(t+1) &= x_i(t) + v_i(t+1) \end{aligned} \tag{28}$$

where $\text{rand}_1, \text{rand}_2 \sim (0, 1)$ introduce stochasticity.

PSO is particularly useful for PID controller tuning, where the search space is defined by the proportional (k_p), integral (k_i), and derivative (k_d) gains. The fitness function evaluates control performance using metrics like rise time, average error, and standard deviation, as shown in Equation (29).

$$\text{Fitness} = k_1 t_r + k_2 \mu_e + k_3 \sigma_e \tag{29}$$

The optimization process follows these steps:

1) Initialize particles with random positions and velocities.
2) Evaluate each particle's fitness based on the objective function.
3) Update p_i and $p_{\text{best},i}$ if a better solution is found.

4) Determine the best-performing particle globally, g_{best}.
5) Adjust velocity and position using the updated equations.
6) Repeat until a stopping criterion is met (maximum iterations or sufficient accuracy).

Although $c_1 = c_2 = 2$ is common, research suggests that $c_1 = c_2 = 1.49$ can improve convergence. Proper tuning accelerates the search while avoiding local minima, leading to efficient controller parameter selection. This is possible by using the PID tuning gains mentioned before and the PSO parameters as shown in Table IV.

TABLE IV. PSO CONTROLLER PARAMETERS AND FITNESS WEIGHT

PSO Controller Parameter	**Value**
No. of Particles (Nc)	50
No. of Iterations (Max Iter)	50
Cognitive Coefficient (c1)	2
Social Coefficient (c2)	2
Fitness Weights	
K1	1
K2	10
K3	100

Using the previous parameters after simulation, it is evident that the output angular velocity oscillates around the setpoint, as the PSO-controlled system initially exhibits oscillations (0–10 sec) as it adjusts, followed by a relatively stable phase (10–25 sec) with minor fluctuations. Around $t = 30$ seconds, large oscillations in $\dot{\alpha}$, like a sudden instability, occur, with an oscillatory spark appearing around it for a period of 2 seconds with a value of $(-6, 8)$ m/s, likely due to system nonlinearities. The system quickly recovers and stabilizes after 35 seconds, then converges and tends to 2. While PSO effectively maintains control for most of the response, Fig. 9 clearly shows the following findings: rise time $t_r = 0.0384$ s, mean value $\mu_e = 2.0206$, standard deviation $\sigma_e = 1.0984$, coefficient of variation $c.v = 35\%$, and error $e = 1.032\%$.

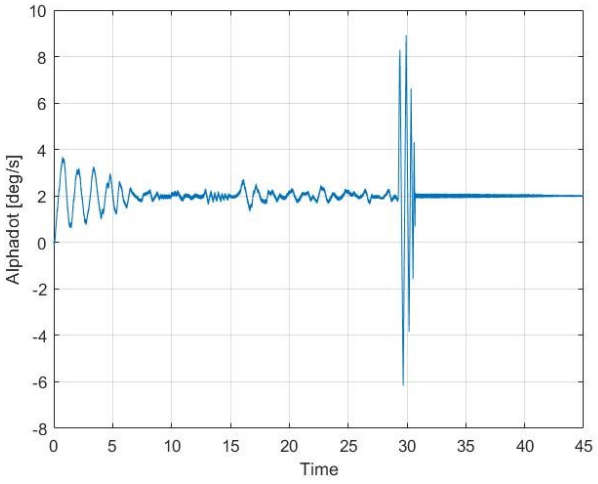

Fig. 9. Step Response Simulation Result of PSO

Fig. 10 illustrates the Particle Swarm Optimization (PSO) algorithm used to optimize the controller gains K_p, K_i, and K_d. The process begins by utilizing a system model and initializing the PSO parameters, including the number of particles ($N_c = 50$), cognitive and social acceleration coefficients ($C_1 = 2$, $C_2 = 2$), and fitness function weights ($k_1 = 1$, $k_2 = 10$, $k_3 = 100$). The number of iterations is set to 50. Each particle's position and velocity are initialized, and their performance is evaluated based on a fitness function. The algorithm iteratively updates particle positions and velocities using Equation (43), tracking the best solution (X_{pbest}). The process continues until the maximum iteration count ($N_C >$ Max_Itr). Once completed, the optimized controller gains (K_p, K_i, and K_d) are outputted in the control system.

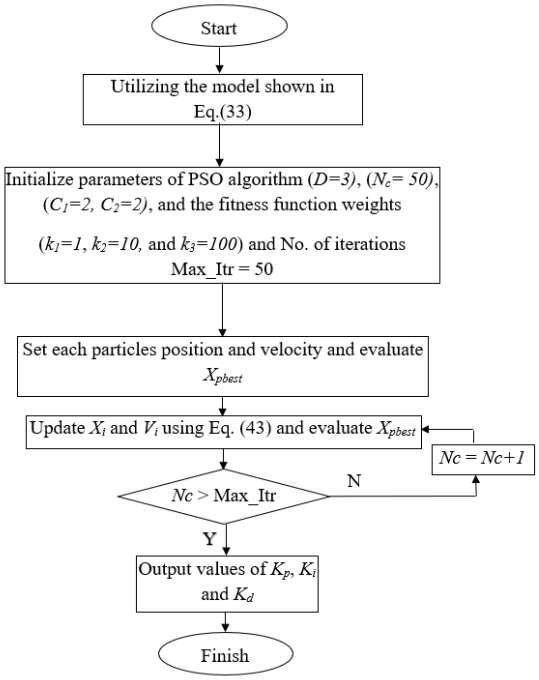

Fig. 10. PSO implementation procedure with erection system

G. System Simulation

The actuation of a nonlinear system is simulated using a proposed control framework that incorporates a classical PID controller and a Sliding Mode Control (SMC) strategy. The results are compared with those obtained from Model Predictive Control (MPC) and a PSO-tuned PID controller. The simulation is conducted in the MATLAB/Simulink environment, integrating the Proportional Directional Control Valve (PDCV) model [65], the hydraulic cylinder model, and relevant control dynamics.

1) Classical Controller Simulation: Fig. 11 presents the simulation of a classical PID controller for angular velocity

control. The system processes feedback from the actual angular velocity and applies a PID-based correction to minimize the error between the commanded and measured values [66]. The simulation is conducted with a reference angular velocity of 2°/s to evaluate the controller's performance.

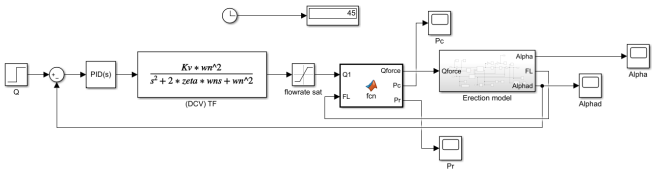

Fig. 11. Classical control simulation

Fig. 12 presents the step response of the classical controller applied to a nonlinear system. The system exhibits an initial transient response with a rise time of $t_r = 0.0384$ seconds. The mean steady-state error is $\mu_e = 0.0034°$, with a standard deviation of $\sigma = 0.1562°$, indicating minor fluctuations around the desired value. The zoomed-in views highlight the response characteristics at different intervals, showcasing initial overshoot, mid-range oscillations, and steady-state behavior.

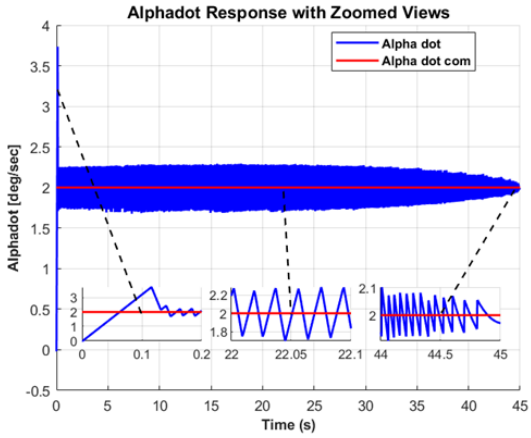

Fig. 12. classical control step response

2) SMC System Simulation: Fig. 13 illustrates the simulation of a (SMC)-based system for regulating the erection mechanism. The objective of the controller is to minimize a predefined cost function while ensuring robustness against system uncertainties and disturbances. SMC is employed due to its ability to enforce robustness through a properly designed sliding surface, ensuring a stable Lyapunov function while minimizing rise time, settling time, and overshoot.

The control strategy leverages angular velocity feedback $\dot{\alpha}$ to regulate the erection beam's motion. By integrating $\dot{\alpha}$, the angular position α is obtained, while differentiation provides the angular acceleration $\ddot{\alpha}$ and its higher derivative $\dddot{\alpha}$, enabling full-state feedback. The Simulink model demonstrates the interaction between the controller, the (PDCV) input, the erection model, and feedback loops, ensuring precise and stable trajectory tracking [67].

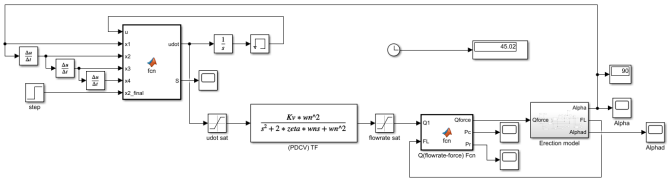

Fig. 13. SMC control simulation

Fig. 14 presents the system's step response under a commanded angular velocity of $\dot{\alpha}_c = 2°/s$. The response exhibits a rapid rise time of $t_r = 0.0454$ s, demonstrating the controller's fast-tracking capability. The mean absolute error is measured at $\mu_e = 0.0323\%$, while the standard deviation is $\sigma_e = 0.1233°/s$, indicating minimal fluctuations around the desired trajectory. The zoomed-in sections highlight transient behaviors at key time intervals, showcasing the system's ability to closely follow the reference input with negligible steady-state error. These results validate the robustness and accuracy of the proposed Sliding Mode Control (SMC) in regulating the erection beam's angular velocity.

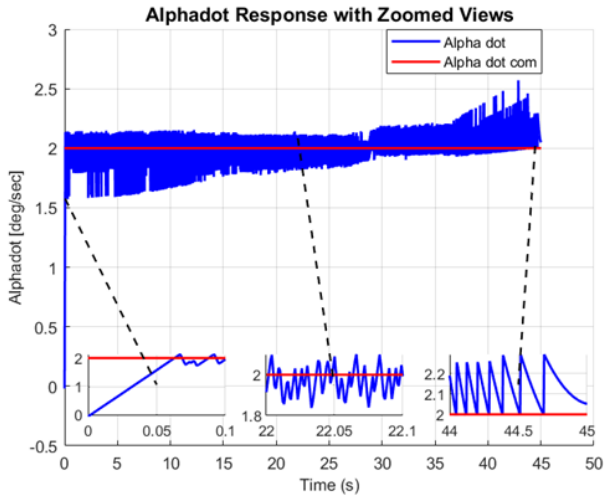

Fig. 14. Step response Simulation result of SMC at $\dot{\alpha}_c = 2\ deg/sec$

TableV presents the selected Sliding Mode Control (SMC) parameters and their corresponding final angular velocity x_3 for different commanded angular accelerations ($\dot{\alpha}_c$). The commanded values are set at 2°/s, 1°/s, 0.5°/s, and 0.25°/s, allowing for a comparative evaluation of the controller's performance across varying input conditions. The table highlights key tuning parameters, including k, c_1, c_2, c_3, c_4, and pp, along with the resulting settling time and rise time (t_r). Notably, the rise time decreases as the commanded angular acceleration increases, demonstrating the control system's responsiveness and adaptability under different operating conditions.

TABLE V. SMC PARAMETERS x_3 FINAL (°/S) WITH RELATION TO INPUT VELOCITIES OF THE NONLINEAR MODEL

$x_{3\text{final}}$ (°/s)	k	c_1	c_2	c_3	c_4	PP	Time	t_r
2	40	0.01	0.08	350	0.2	1	45.02	0.055
1	100	0.09	0.001	600	0.3	0.7	98.998	0.025
0.5	55	0.05	0.001	250	0.03	1.3	189.236	0.011
0.25	300	0.01	0.01	750	0.57	1	360.084	0.006

Fig. 15 illustrates the system's step response under different angular acceleration inputs, providing a visual representation of the controller's effectiveness in tracking the desired reference. Each subplot corresponds to a specific input acceleration, depicting the system's transient and steady-state behavior. The zoomed-in sections offer insight into key performance metrics, such as rise time, steady-state error, and oscillatory behavior. As observed, higher input accelerations result in faster rise times and shorter response durations, while lower input accelerations exhibit more pronounced oscillations before settling. These findings validate the robustness of the SMC approach in maintaining precise tracking performance across varying input conditions.

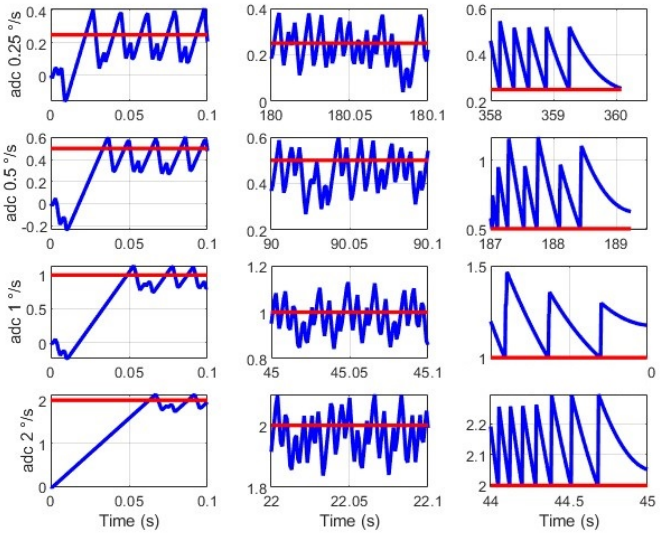

Fig. 15. Step response simulation result of SMC at different angular velocities

Fig. 16 illustrates the step response of the SMC system for different commanded angular velocities. The plot shows how the angle α evolves over time under different input velocity conditions (0.25°/s, 0.5°/s, 1°/s, and 2°/s). The curves indicate the system's response, with higher input velocities resulting in a steeper slope, demonstrating the effect of velocity inputs on the angular position over time.

III. RESULTS AND DISCUSSION

A. Verification of Control Algorithms

The non-linear system shown in Fig. 17 is accompanied by a classical control algorithm, SMC synthesis, MPC system, and PID-PSO system. Hereinafter, the simulations are carried out for reference commanded angular velocities 0.25 °/s, 0.5 °/s, 1 °/s, and 2 °/s, as they will be the settled velocities for beam erection [68].

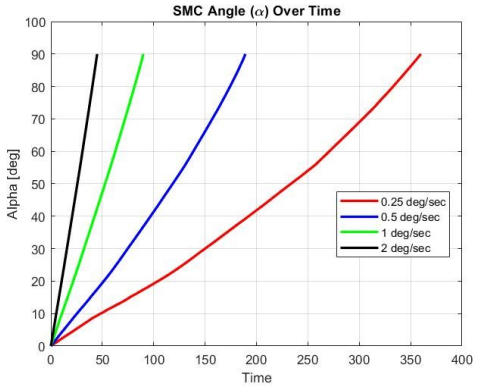

Fig. 16. Step response Simulation result of SMC at different angular velocities (alpha with time)

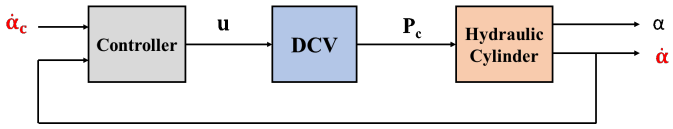

Fig. 17. Simulation Block Diagram of the Control System for Beam Erection

To assess the performance of different control strategies, statistical data from sixteen simulations were analyzed. Table VI summarizes key performance metrics, including the average error and standard deviation for each method. These metrics provide insights into the stability and accuracy of each controller. Additionally, Fig. 18 visualizes the average velocity achieved by the control techniques, allowing for a comparative evaluation of their effectiveness.

Fig. 18 provides a graphical representation of the average velocity values for each control method. The results reinforce the effectiveness of SMC, as it closely tracks the desired velocity with minimal deviations. These findings indicate that SMC not only ensures more accurate velocity regulation but also requires less control effort, making it a favorable choice for applications demanding high stability and precision.

Similarly, Table VI highlights that the SMC system consistently achieves the lowest average error and standard deviation among all tested control techniques. Compared to the classical controller, MPC, and PID-PSO systems, SMC demonstrates superior precision and robustness across all four target angular velocities. The reduced variability in performance suggests that SMC maintains better control stability while minimizing fluctuations.

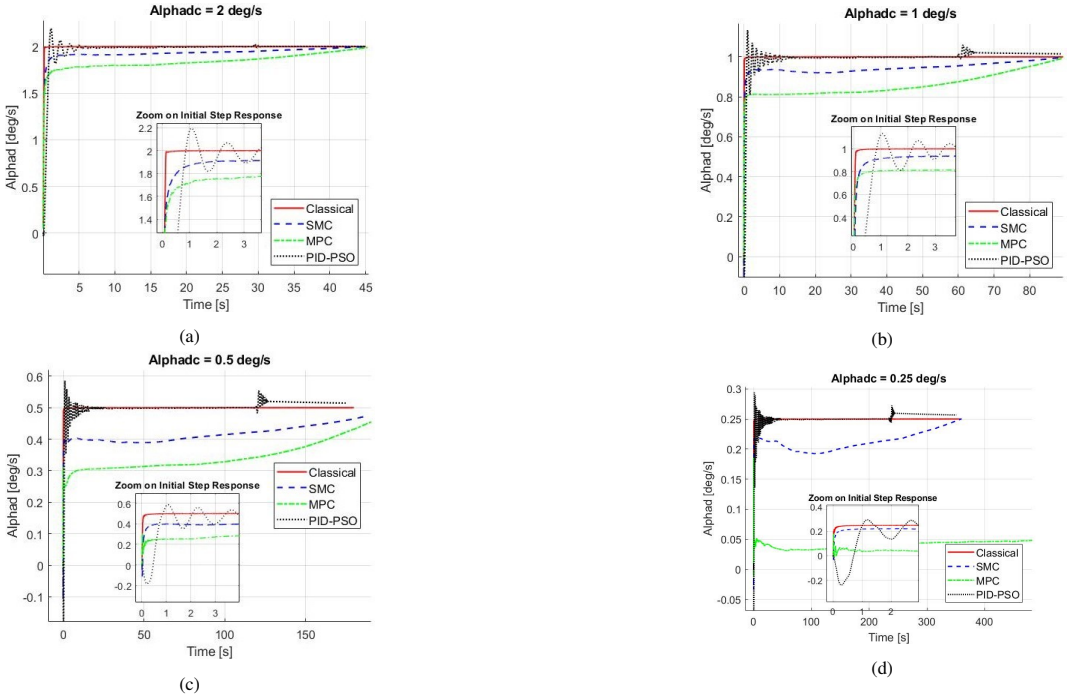

Fig. 18. Average Velocity values for control Techniques

TABLE VI. CONTROLLER PERFORMANCE FOR DIFFERENT COMMANDED ANGULAR VELOCITIES

$\dot{\alpha}$ (°/s)	Controller	Rise time t_r (Sec)	Mean (m) °/s	S_d (σ) °/s	Coeff of var (c.v) %	Average error (μ_e) %	Simulation time (sec)
2	PID	0.0384	2.0001	0.1562	7.8113	0.0034	44.998
	SMC	0.0454	1.9994	0.1233	6.1695	0.0323	45.021
	MPC	0.0414	1.9889	0.2776	13.9567	0.5568	45.252
	PID-PSO	0.3845	2.0206	1.0984	54.36	1.0321	44.542
1	PID	0.0265	1.0000	0.1447	14.4705	0.0013	89.999
	SMC	0.0264	1.0003	0.1160	11.5979	0.0311	89.998
	MPC	0.0047	0.9988	0.2544	25.4673	0.1237	90.111
	PID-PSO	0.3255	1.0154	1.4847	146.2193	1.5398	88.642
0.5	PID	0.0128	0.5001	0.1440	28.8031	0.0141	179.974
	SMC	0.0119	0.4759	0.1241	26.0674	4.8163	189.236
	MPC	0.0128	0.4631	0.2438	52.6403	7.3831	194.345
	PID-PSO	0.1514	0.5145	1.6700	324.5805	2.9043	174.943
0.25	PID	0.0031	0.2500	0.1441	57.6368	0.0030	359.987
	SMC	0.0024	0.2503	0.1041	41.5864	0.1236	360.084
	MPC	0.0057	0.1279	0.2248	175.8245	48.8525	703.747
	PID-PSO	0.0013	0.2567	1.0355	403.3781	2.6867	350.728

B. Verification of Control Algorithms under Disturbed conditions

To evaluate the robustness of the control algorithms, the system is subjected to external disturbances. A force disturbance is applied to the nonlinear model for a short duration, while white noise is introduced into the angular velocity feedback. The following figures illustrate these disturbances in the simulation environment.

Fig. 19 illustrates the sensor noise introduced into the angular velocity feedback. The white noise simulates real-world sensor imperfections, ensuring that the control algorithm can operate effectively under noisy conditions. The noise fluctuates within a range of approximately $\pm 1°$/s, introducing measurement uncertainties that the controller must compensate for.

The force disturbance applied to the system is represented in Fig. 20. A sudden increase in force of 20.75 kN is introduced at $t = 20$ s, lasting for 3 seconds before returning to zero. This disturbance aims to assess the controller's ability to reject external forces and maintain stability. These disturbances provide a realistic testing scenario to verify the system's stability and robustness against external influences.

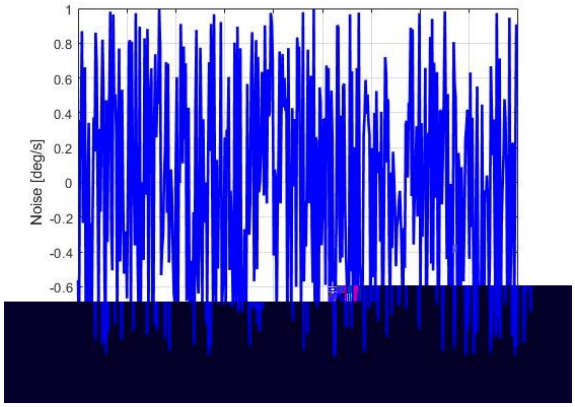

Fig. 19. Sensor noise

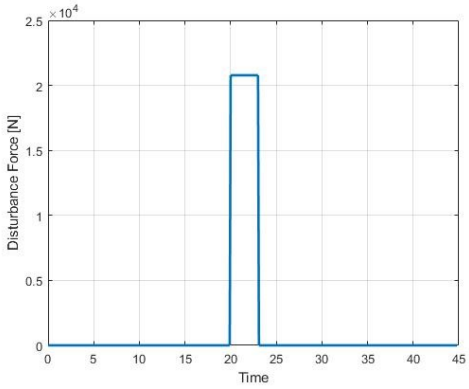

Fig. 20. Disturbance force

Fig. 21 presents the simulation block diagram of the system under external disturbances. A pressure disturbance of +5 bar is applied to the hydraulic cylinder input to assess the system's ability to handle variations in actuation pressure. Additionally, Gaussian random noise, constrained within ±1°/s, is introduced into the angular velocity sensor (as shown in Fig. 19 to evaluate the controller's robustness against sensor measurement uncertainties.

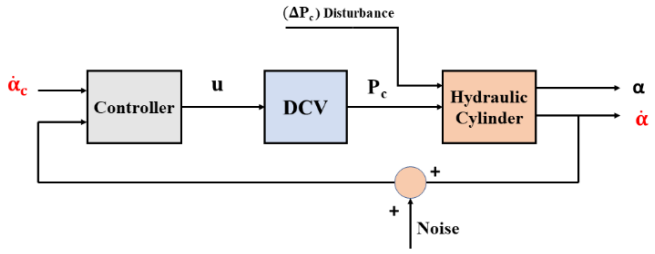

Fig. 21. Simulation block diagram for the disturbed system

1) Comparison of Control Techniques under Disturbances: In practical control systems, external disturbances and noise can significantly affect system performance. To evaluate the robustness of different control techniques, disturbances were introduced into the system at various levels of commanded angular velocity $\dot{\alpha}_{dc}$. The results for four control strategies—Classical, SMC, MPC, and PID-PSO—are presented in the following comparative analysis. The response of each controller is analyzed based on its ability to maintain stability, minimize errors, and achieve a smooth response under disturbed conditions.

Fig. 22 illustrates the response of each control technique for different disturbance levels of $\dot{\alpha}_{dc}$ (2°/s, 1°/s, 0.5°/s, and 0.25°/s). The results indicate that while all controllers respond to disturbances, the SMC method exhibits superior robustness. Specifically, the SMC's mean error and standard deviation remain relatively unchanged across different disturbance levels. In contrast, the Classical, MPC, and PID-PSO controllers exhibit significant increases in mean error and variability, highlighting their sensitivity to disturbances.

The inset zoomed-in views provide a closer examination of the initial step response for each case, revealing transient behaviors and overshoot characteristics. The robustness of the SMC approach is further emphasized as it maintains a consistent response with minimal variations compared to the other controllers.

A detailed statistical analysis of the control system's performance under disturbances is provided in Table VII. This table presents key performance metrics such as rise time, mean response, standard deviation, coefficient of variation, average error, and simulation time. The data further reinforces the robustness of SMC, which maintains low variability and error across different disturbance levels.

Compared to other controllers, SMC consistently exhibits the smallest standard deviation and coefficient of variation, signifying higher stability and reliability. In contrast, the PID-PSO controller, despite its optimization-based tuning, shows high sensitivity to disturbances, leading to large errors and deviations.

IV. Conclusions

This study explores control methodologies for regulating the angular velocity of beam erection, aiming to precisely control the time required for the full erection of a launch vehicle's beam. The control system is developed using four approaches: classical control, Sliding Mode Control (SMC), Model Predictive Control (MPC), and a Particle Swarm Optimization-tuned Proportional-Integral-Derivative (PSO-PID) controller. The nonlinear dynamics of the erection system are first derived and then linearized to facilitate controller design. The classical and SMC controllers are designed using the linearized system and subsequently tested on the nonlinear model, whereas the MPC and PSO-PID controllers are designed and simulated directly on the nonlinear system.

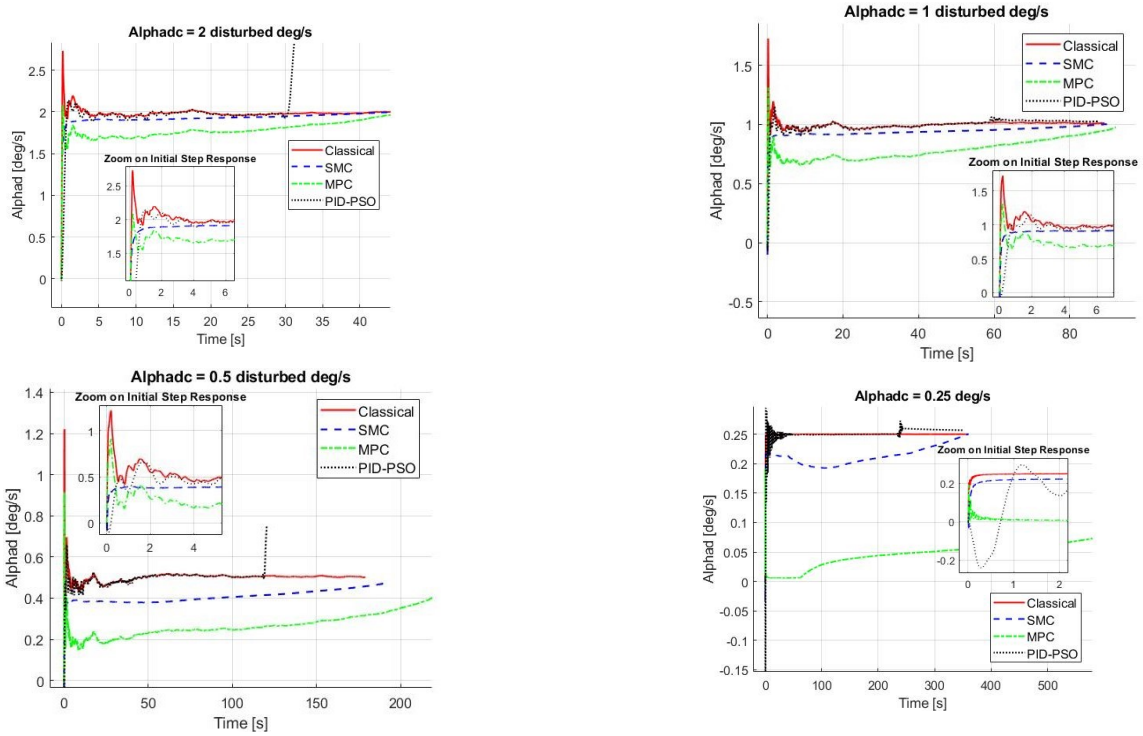

Fig. 22. Average velocity values for control techniques in the presence of noise and disturbance

TABLE VII. STATISTICAL DATA FOR DISTURBED CONTROL SYSTEM SIMULATIONS

$\dot{\alpha}$ (°/s)	Controller	Rise time t_r (Sec)	Mean (m) °/s	S_d (σ) °/s	Coeff of var (c.v) %	Average error (μ_e) %	Simulation time (sec)
2	PID	0.0384	2.0051	0.6598	32.9076	0.2537	44.887
	SMC	0.0454	1.9992	0.1378	6.891	0.0388	45.023
	MPC	0.0507	1.9897	0.6447	32.4007	0.5163	45.235
	PID-PSO	0.0020	2.8661	5.3033	185.0392	43.3026	31.415
1	PID	0.0188	1.0093	0.6599	65.3854	0.9267	89.173
	SMC	0.0153	1.0018	0.1292	12.8953	0.1760	89.864
	MPC	0.0188	0.9764	0.6305	64.5799	2.3637	92.179
	PID-PSO	0.0008	1.0252	1.3502	131.6991	2.5216	87.802
0.5	PID	0.0188	0.5027	0.6569	130.684	0.5306	179.052
	SMC	0.0119	0.4722	0.1379	29.2104	5.5542	190.713
	MPC	0.0008	0.4091	0.6223	152.1284	18.1815	219.997
	PID-PSO	0.0029	0.7478	2.5069	335.2266	49.566	120.419
0.25	PID	0.0246	0.2574	0.6626	257.3751	2.9736	349.604
	SMC	0.0024	0.2481	0.1130	45.5407	0.7596	363.258
	MPC	0.0095	-0.0521	0.5888	-1130.4	120.8339	inf
	PID-PSO	0.0334	0.2725	1.4717	540.128	8.9916	330.534

Simulation results indicate that SMC achieves the lowest average error and standard deviation in the controlled parameters, implying minimal control effort. Under sensor noise and external disturbances, SMC maintains its performance with only a slight change in mean error and standard deviation, demonstrating superior robustness compared to other techniques. While direct comparison with real-world data is not yet feasible, the model has been rigorously validated against established theoretical frameworks and data from similar systems. Future research will focus on experimental validation through industry collaboration and laboratory testing to further confirm the model's reliability in practical applications. This will enable a deeper analysis of its safety, precision, and efficiency in hydraulic and mechanical systems.

REFERENCES

[1] M. Hu and Y. Jiang, "Research on the high speed of piston pumps based on rapid erecting of launch vehicles," *Applied Sciences*, vol. 13, no. 12, 2023, doi: 10.3390/app13127178.

[2] Z. Luo, J. Wang, J. Wu, S. Zhang, Z. Chen, and B. Xie, "Research on a hydraulic cylinder pressure control method for efficient traction operation in electro-hydraulic hitch system of electric tractors," *Agriculture*, vol. 13, no. 8, 2023, doi: 10.3390/agriculture13081555.

[3] T. A. Nguyen, "Using a novel fuzzy 3-inputs algorithms to control the active hydraulic stabilizer bar with the complex model of the vehicle nonlinear dynamics," *PLoS One*, vol. 18, no. 3, 2023, doi: 10.1371/journal.pone.0282505.

[4] C. Jing, H. Zhang, B. Yan, Y. Hui, and H. Xu, "State and disturbance observer based robust disturbance rejection control for friction electro-hydraulic load simulator," *Nonlinear Dynamics*, vol. 112, no. 19, pp. 17241–17255, 2024, doi: 10.1007/s11071-024-09935-8.

[5] J. Liu, C. Yuan, L. Matias, C. Bowen, V. Dhokia, M. Pan, and J. Roscow, "Sensor technologies for hydraulic valve and system performance monitoring: Challenges and perspectives," *Advanced Sensor Research*, vol. 3, no. 7, 2024, doi: 10.1002/adsr.202300130.

[6] B. Yi, Y. Zhan, and J. Xu, "Dynamic analysis and optimization of a novel dual-valve heave compensator for heavy lifting operations," *Ocean Engineering*, vol. 309, 2024, doi: 10.1016/j.oceaneng.2024.118528.

[7] M. H. Nguyen, H. V. Dao, and K. K. Ahn, "Extended sliding mode observer-based high-accuracy motion control for uncertain electro-hydraulic systems," *International journal of robust and nonlinear control*, vol. 33, no. 2, pp. 1351–1370, 2023, doi: 10.1002/rnc.6421.

[8] M. Ali *et al*., "Enhanced hybrid robust fuzzy-pid controller for precise trajectory tracking electro-hydraulic actuator system," *International Journal of Robotics & Control Systems*, vol. 4, no. 2, pp. 795–813, 2024, doi: 10.31763/ijrcs.v4i2.1407.

[9] M. Iskandar, C. Ott, A. Albu-Schäffer, B. Siciliano and A. Dietrich, "Hybrid Force-Impedance Control for Fast End-Effector Motions," in *IEEE Robotics and Automation Letters*, vol. 8, no. 7, pp. 3931-3938, 2023, doi: 10.1109/LRA.2023.3270036.

[10] J. Li, L. Kong, H. Liang, and W. Li, "Review of development and characteristics research on electro-hydraulic servo system," *Recent Patents on Engineering*, vol. 18, no. 6, pp. 140–154, 2024, doi: 10.2174/1872212118666230711165517.

[11] I. Lopez-Sanchez and J. Moreno-Valenzuela, "Pid control of quadrotor uavs: A survey," *Annual Reviews in Control*, vol. 56, 2023, doi: 10.1016/j.arcontrol.2023.100900.

[12] A. Mohammadzadeh, M. H. Sabzalian, C. Zhang, O. Castillo, R. Sakthivel, and F. F. El-Sousy, *Modern Adaptive Fuzzy Control Systems*, Springer Cham, 2023, doi: 10.1007/978-3-031-17393-6.

[13] F. Menzri, T. Boutabba, I. Benlaloui, H. Bawayan, M. I. Mosaad, and M. M. Mahmoud, "Applications of hybrid smc and flc for augmentation of mppt method in a wind-pv-battery configuration," *Wind Engineering*, vol. 48, no. 6, pp. 1186–1202, 2024, doi: 10.1177/0309524X241254364.

[14] D. Wang, W. Xiao, J. Shao, M. Li, Y. Zhao, and Y. Jiang, "Rolling mechanism of launch vehicle during the prelaunch phase in sea launch," *Aerospace*, vol. 11, no. 5, 2024, doi: 10.3390/aerospace11050399.

[15] Z. Duan, C. Sun, J. Li, and Y. Tan, "Research on servo valve-controlled hydraulic motor system based on active disturbance rejection control," *Measurement and Control*, vol. 57, no. 2, pp. 113–123, 2024, doi: 10.1177/00202940231194115.

[16] D. Liu, X. Zong, Y. Zhao, Z. Jiang, and D. Cheng, "Trajectory planning and control strategy optimization design of double electric cylinder erecting device," in *Journal of Physics: Conference Series*, vol. 2764, no. 1, 2024, doi: 10.1088/1742-6596/2764/1/012070.

[17] M. Ledvoň, L. Hružík, A. Bureček, F. Dỳrr, and T. Polášek, "Leakage characteristics of proportional directional valve," *Processes*, vol. 11, no. 2, 2023, doi: 10.3390/pr11020512.

[18] M. Y. Salloom and M. Y. Almuhanna, "Analysis of the improved proportional hydraulic directional control valve by adding a solenoid directional valve," *Journal Européen des Systèmes Automatisés*, vol. 57, no. 1, pp. 105–115, 2024, doi: 10.18280/jesa.570111.

[19] Y. Li, R. Li, J. Yang, X. Yu, and J. Xu, "Review of recent advances in the drive method of hydraulic control valve," *Processes*, vol. 11, no. 9, 2023, doi: 10.3390/pr11092537.

[20] S. Jiang, F. Huang, W. Liu, Y. Huang and Y. Chen, "A Double Closed-Loop Digital Hydraulic Cylinder Position System Based on Global Fast Terminal Sliding Mode Active Disturbance Rejection Control," in *IEEE Access*, vol. 12, pp. 80138-80152, 2024, doi: 10.1109/ACCESS.2024.3408829.

[21] E. C. Mellquist, A. M. Kabe, V. K. Goyal, and J. Strizzi, "Observations and lessons learned on integrated structural launch and ascent loads and pogo stability analysis requirements," in *AIAA SCITECH 2024 Forum*, 2024, doi: 10.2514/6.2024-1846.

[22] B. Demircan, S. Bıçakçı, and E. Akyüz, "Position control of hydraulic servo cylinder for wave channel," *Konya Journal of Engineering Sciences*, vol. 13, no. 1, pp. 260–276, 2025, doi: 10.36306/konjes.1571870.

[23] Z. Xu, C. Sun, X. Hu, Q. Liu and J. Yao, "Barrier Lyapunov Function-Based Adaptive Output Feedback Prescribed Performance Controller for Hydraulic Systems With Uncertainties Compensation," in *IEEE Transactions on Industrial Electronics*, vol. 70, no. 12, pp. 12500-12510, 2023, doi: 10.1109/TIE.2023.3236114.

[24] F. Sciatti, P. Tamburrano, E. Distaso, and R. Amirante, "Digital hydraulic valves: Advancements in research," *Heliyon*, vol. 10, no. 5, 2024, doi: 10.1016/j.heliyon.2024.e27264.

[25] A. S. Samosir, T. Sutikno, and L. Mardiyah, "Simple formula for designing the pid controller of a dc-dc buck converter," *International Journal of Power Electronics and Drive Systems*, vol. 14, no. 1, pp. 327–336, 2023, doi: 10.11591/ijpeds.v14.i1.pp327-336.

[26] J. Ansari, M. Homayounzade, and A. R. Abbasi, "Load frequency control in power systems by a robust backstepping sliding mode controller design," *Energy Reports*, vol. 10, pp. 1287–1298, 2023, doi: 10.1016/j.egyr.2023.08.008.

[27] A. Norouzi, H. Heidarifar, H. Borhan, M. Shahbakhti, and C. R. Koch, "Integrating machine learning and model predictive control for automotive applications: A review and future directions," *Engineering Applications of Artificial Intelligence*, vol. 120, 2023, doi: 10.1016/j.engappai.2023.105878.

[28] N. H. Sahrir and M. A. M. Basri, "Pso–pid controller for quadcopter uav: index performance comparison," *Arabian Journal for Science and Engineering*, vol. 48, no. 11, pp. 15241–15255, 2023, doi: 10.1007/s13369-023-08088-x.

[29] Y. Wang, C. Shen, J. Huang, and H. Chen, "Model-free adaptive control for unmanned surface vessels: A literature review," *Systems Science & Control Engineering*, vol. 12, no. 1, 2024, doi: 10.1080/21642583.2024.2316170.

[30] Y. Wang and S. Salehi, "Application of real-time field data to optimize drilling hydraulics using neural network approach," *Journal of Energy Resources Technology*, vol. 137, no. 6, 2015, doi: 10.1115/1.4030847.

[31] M. A. Abuhussain, B. S. Alotaibi, M. S. Aliero, M. Asif, M. A. Alshenaifi, and Y. A. Dodo, "Adaptive hvac system based on fuzzy controller approach," *Applied Sciences*, vol. 13, no. 20, 2023, doi: 10.3390/app132011354.

[32] Ş. Çetin and A. V. Akkaya, "Simulation and hybrid fuzzy-pid control for positioning of a hydraulic system," *Nonlinear Dynamics*, vol. 61, pp. 465–476, 2010, doi: 10.1007/s11071-010-9662-1.

[33] B. Ning, Y. Zhao, and S. Cheng, "An improved sensorless hybrid control method of permanent magnet synchronous motor based on i/f startup," *Sensors*, vol. 23, no. 2, 2023, doi: 10.3390/s23020635.

[34] H. Razmjooei, G. Palli, E. Abdi, M. Terzo, and S. Strano, "Design and experimental validation of an adaptive fast-finite-time observer on uncertain electro-hydraulic systems," *Control Engineering Practice*, vol. 131, 2023, doi: 10.1016/j.conengprac.2022.105391.

[35] J. -X. Zhang, K. -D. Xu and Q. -G. Wang, "Prescribed Performance Tracking Control of Time-Delay Nonlinear Systems With Output Constraints," in *IEEE/CAA Journal of Automatica Sinica*, vol. 11, no. 7, pp. 1557-1565, 2024, doi: 10.1109/JAS.2023.123831.

[36] Z. Wang, M. Becker, G. Kondla, H. Gimpel, A. L. Beer, and M. W. Greenlee, "Dynamic modulation of the processing of unpredicted technical errors by the posterior cingulate and the default mode network," *Scientific Reports*, vol. 14, no. 1, 2024, doi: 10.1038/s41598-024-64409-6.

[37] H. Razmjooei, G. Palli, F. Janabi-Sharifi, and S. Alirezaee, "Adaptive fast-finite-time extended state observer design for uncertain electro-hydraulic systems," *European Journal of Control*, vol. 69, 2023, doi: 10.1016/j.ejcon.2022.100749.

[38] X. Zhao, X. Zhu, J. Liu, Y. Hu, T. Gao, L. Zhao, J. Yao, and Z. Liu, "Model-assisted multi-source fusion hypergraph convo-

lutional neural networks for intelligent few-shot fault diagnosis to electro-hydrostatic actuator," *Information Fusion*, vol. 104, 2024, doi: 10.1016/j.inffus.2023.102186.

[39] T. Ma, X. Guo, G. Su, H. Deng, and T. Yang, "Research on synchronous control of active disturbance rejection position of multiple hydraulic cylinders of digging-anchor-support robot," *Sensors*, vol. 23, no. 8, 2023, doi: 10.3390/s23084092.

[40] Y. Liu, W. Li, S. Lin, X. Zhou, and Y. Ge, "Hydraulic system fault diagnosis of the chain jacks based on multi-source data fusion," *Measurement*, vol. 217, 2023, doi: 10.1016/j.measurement.2023.113116.

[41] Y. Zhao, H. Wang, B. Song, P. Xue, W. Zhang, S. Peth, R. L. Hill, and R. Horn, "Characterizing uncertainty in process-based hydraulic modeling, exemplified in a semiarid inner mongolia steppe," *Geoderma*, vol. 440, 2023, doi: 10.1016/j.geoderma.2023.116713.

[42] D. Li, N. Dai, H. Wang, and F. Zhang, "Mathematical modeling study of pressure loss in the flow channels of additive manufacturing aviation hydraulic valves," *Energies*, vol. 16, no. 4, 2023, doi: 10.3390/en16041788.

[43] V. Bakırcıoğlu, M. A. Şen, and M. Kalyoncu, "Numerical investigation and experimental verification of the proposed robot leg virtual model," *Proceedings of the Institution of Mechanical Engineers, Part C: Journal of Mechanical Engineering Science*, vol. 236, no. 13, pp. 7426–7441, 2022, doi: 10.1177/09544062221076769.

[44] H. Sun, J. Tao, C. Qin, H. Yu, S. Xu, Q. Zhuang, and C. Liu, "Optimal energy consumption and response capability assessment for hydraulic servo systems containing counterbalance valves," *Journal of Mechanical Design*, vol. 145, no. 5, 2023, doi: 10.1115/1.4056497.

[45] P. Zhang, Y. Tao, C. Yang, W. Ma, and Z. Zhang, "Transient characteristics simulation and flow-field analysis of high-pressure pneumatic pilot-driven on/off valve via cfd method," *Flow Measurement and Instrumentation*, vol. 97, 2024, doi: 10.1016/j.flowmeasinst.2024.102620.

[46] W. Fu, W. Lu, H. Liu, X. Yuan, and D. Zeng, "Smooth braking control of excavator hydraulic load based on command reshaping," *ISA transactions*, vol. 158, pp. 674–685, 2025, doi: 10.1016/j.isatra.2025.01.006.

[47] Y. Yin, D. Wang, J. Fu, and H.-c. Jian, "Effect of dynamic pressure feedback orifice on stability of cartridge-type hydraulic pilot-operated relief valve," *Chinese Journal of Mechanical Engineering*, vol. 36, no. 85, 2023, doi: 10.1186/s10033-023-00922-5.

[48] Z. Qin, Y.-T. Wu, L. He, X. Gao, and S.-K. Lyu, "Empirical research on the friction behavior of o-rings in hydraulic cylinders," *PLoS One*, vol. 18, no. 1, 2023, doi: 10.1371/journal.pone.0280815.

[49] M. Kiani-Oshtorjani, A. Mikkola, and P. Jalali, "Novel bulk modulus model to estimate stiffness in fluid power systems," *Mechatronics*, vol. 92, 2023, doi: 10.1016/j.mechatronics.2023.102987.

[50] S. Osterland, L. Günther, and J. Weber, "Experiments and computational fluid dynamics on vapor and gas cavitation for oil hydraulics," *Chemical Engineering & Technology*, vol. 46, no. 1, pp. 147–157, 2023, doi: 10.1002/ceat.202200465.

[51] Y. Shen, Y.-Q. Guo, X. Zha, and Y. Wang, "Real-time hybrid test control research based on improved electro-hydraulic servo displacement algorithm," *Sensors*, vol. 23, no. 10, 2023, doi: 10.3390/s23104765.

[52] I. H. A. Al-Hady, F. M. Mohammed, and J. A. Mohammed, "Modeling and simulation of telescopic hydraulic for elevating purposes," *Engineering and Technology Journal*, vol. 40, no. 01, pp. 226–232, 2022, doi: 10.30684/etj.v40i1.2253.

[53] K. K. Sahu and V. K. Gupta, "Effect of wear rings on buckling load capacity of two-stage hydraulic cylinder," in *Structures*, vol. 50, 2023, pp. 1965–1979, doi: 10.1016/j.istruc.2023.02.114.

[54] V. Ding, S. Torabian, X. Yun, A. Pervizaj, S. Madsen, and B. Schafer, "Experimental investigation of buckling of thin-walled cylindrical shells subjected to combined bending and torsion," in *Proceedings of the Annual Stability Conference Structural Stability Research Council Charlotte, North Carolina*, 2022.

[55] A. K. Kumawat, R. Rout, R. Kumawat, and M. Rawat, "Discrete-time constrained controller for proportional directional control valve-based electrohydraulic system with parametric uncertainty and disturbances," *Journal of Dynamic Systems, Measurement, and Control*, vol. 145, no. 7, 2023, doi: 10.1115/1.4062469.

[56] H. Wang, T. Zou, H. Zheng, Z. Yang, and J. Wang, "A double-layer model predictive control algorithm for valve position control systems," *Proceedings of the Institution of Mechanical Engineers, Part I: Journal of Systems and Control Engineering*, vol. 237, no. 3, pp. 539–550, 2023, doi: 10.1177/09596518221127506.

[57] H. Su, C. Yang, T. Yu and Y. Shang, "Honing tool system development of electro-hydraulic servo valve based on adaptive pressure control," *CSAA/IET International Conference on Aircraft Utility Systems (AUS 2024)*, pp. 699-704, 2024, doi: 10.1049/icp.2024.2973.

[58] J. H. Mohmmed, A. K. Hassan, M. Ali, S. A. Kokz, M. H. Mosa, A. Kareem, A. A. Zainulabdeen, and Z. Feng, "Design of uncertain displacement controlled velocity control system for hydraulic actuator," *Heliyon*, vol. 10, no. 4, 2024.

[59] X. Sun, J. Fu, H. Yang, M. Xie, and J. Liu, "An energy management strategy for plug-in hybrid electric vehicles based on deep learning and improved model predictive control," *Energy*, vol. 269, 2023, doi: 10.1016/j.energy.2023.126772.

[60] L. Cecchin, T. Ohtsuka, A. Trachte, and M. Diehl, "Model predictive controller for hydraulic cylinders with independent metering control valves," *IFAC-PapersOnLine*, vol. 58, no. 18, pp. 281–287, 2024, doi: 10.1016/j.ifacol.2024.09.044.

[61] K. Hu and K. Cheng, "Trajectory planning for an articulated tracked vehicle and tracking the trajectory via an adaptive model predictive control," *Electronics*, vol. 12, no. 9, 2023, doi: 10.3390/electronics12091988.

[62] Y. Zheng, R. Sun, F. Li, Y. Liu, R. Song, and Y. Li, "Parameter identification and position control for helical hydraulic rotary actuators based on particle swarm optimization," *Mechatronics*, vol. 94, 2023, doi: 10.1016/j.mechatronics.2023.103006.

[63] Y. Yu, R. Zeng, Y. Xue, and X. Zhao, "Optimization strategy of rolling mill hydraulic roll gap control system based on improved particle swarm pid algorithm," *Biomimetics*, vol. 8, no. 2, 2023, doi: 10.3390/biomimetics8020143.

[64] X. Liu, Z. Shan, F. Yang and J. Li, "Research on Key Problems of Synchronous Control of Hydraulic System Based on Particle Swarm Fuzzy PID," *2023 IEEE International Conference on Mechatronics and Automation (ICMA)*, pp. 1732-1737, 2023, doi: 10.1109/ICMA57826.2023.10215646.

[65] S. Jaiswal, J. Sopanen, and A. Mikkola, "Efficiency comparison of various friction models of a hydraulic cylinder in the framework of multibody system dynamics," *Nonlinear Dynamics*, vol. 104, no. 4, pp. 3497–3515, 2021, doi: 10.1007/s11071-021-06526-9.

[66] M. Y. Coskun and M. İtik, "Intelligent pid control of an industrial electro-hydraulic system," *ISA transactions*, vol. 139, pp. 484–498, 2023, doi: 10.1016/j.isatra.2023.04.005.

[67] R. Wang, H. t. Liu and X. Xing, "A novel full-state feedback control combined FTO and SMC of electro-hydraulic systems," *2023 China Automation Congress (CAC)*, pp. 3450-3455, 2023, doi: 10.1109/CAC59555.2023.10451680.

[68] M. Z. Fadel, "Hybrid control algorithm sliding mode-pid for an electrohydraulic servo actuator system based on particle swarm optimization technique," *International Information and Engineering Technology Association*, vol. 56, no. 1, pp. 153–163, 2023, doi: 10.18280/jesa.560119.